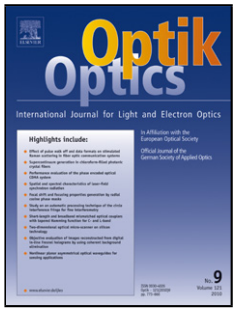

EUV multilayer mirrors in solar X-EUV Imager

Haifeng Wang, Xiaodong Wang, Bo Chen, Yunqi Wang, Shilei Mao, Shuai Ren, Peng Zhou, Yang Liu, Tonglin Huo, Hongjun Zhou

PII: S0030-4026(20)30047-4

DOI: https://doi.org/10.1016/j.ijleo.2020.164213

Reference: IJLEO 164213

To appear in: *Optik*

Received Date: 8 April 2019

Revised Date: 24 December 2019

Accepted Date: 11 January 2020

Please cite this article as: Wang H, Wang X, Chen B, Wang Y, Mao S, Ren S, Zhou P, Liu Y, Huo T, Zhou H, EUV multilayer mirrors in solar X-EUV Imager, *Optik* (2020), doi: https://doi.org/10.1016/j.ijleo.2020.164213

EUV multilayer mirrors in solar X-EUV Imager

Haifeng Wang[1], Xiaodong Wang[1,*], Bo Chen[1], Yunqi Wang[1], Shilei Mao[1], Shuai Ren[1], Peng Zhou[1], Yang Liu[1], Tonglin Huo[2], Hongjun Zhou[2]

[1]*State Key Laboratory of Applied Optics, Changchun Institute of Optics, Fine Mechanics and Physics, Chinese Academy of Sciences, Changchun 130033, China*
[2]*National Synchrotron Radiation Laboratory, University of Science and Technology of China, Hefei 230026, China*
*wangxiaodong@ciomp.ac.cn

Abstract

Fe XII line (19.5 nm) is one of important targets of imaging detection in solar spectrum, and 19.5 nm multilayer mirrors were employed to reflect 19.5 nm line and suppress sidelobe. 19.5 nm multilayer mirrors with a bandwidth of 1.0 nm are in demand in Solar X-EUV imager installed in FengYun III satellite. Thickness ratios of Mo layer of 0.15 and 0.11, respectively, are utilized in multilayer mirrors at normal and 45° incidence. The influence of roughness/diffusion on reflectance is discussed, and profile changes of substrate after deposition are also analyzed.

Keywords: 19.5 nm, Mo/Si, Stress.

1 Introduction

It is an important question to understand the solar-terrestrial environment and its effect on global weather and climate of the Earth. Solar flare, coronal mass ejection are important factors that influence global weather and climate of the Earth. Thus, people did a lot of imaging research on extreme ultraviolet (EUV) emission lines in solar spectrum [1-7]. Two kinds of optical systems are often employed. One is single-spherical-mirror system, the other is two-mirror Cassegrain-type system. The former was utilized in TEX Onboard SELENE of Japan [6] and extreme-ultraviolet camera [7] onboard Chang E lunar Lander. The latter was widely used in SUVI [4] of GOES-R, AIA [5] of SDO, and EIT [2]. There are a primary concave mirror with a central hole and a secondary convex mirror in Cassegrain optical system. The mirror profiles can be aspheric surface (paraboloid, hyperboloid, ellipsoid) and sphere. Solar X ray and EUV (X-EUV) imager is developed by our group. We utilize spherical Cassegrain optical system, and detection target is XII line (19.5 nm) of Fe element.

XII line (19.5 nm) of Fe element is one of important targets of imaging detection in solar spectrum. Instruments, such as TXI, EIT [2], TRACE [3], SUVI [4], and AIA [5], conducted Fe XII line imaging detection. To achieve high spectral purity, the mirror is required to have a narrow bandwidth as well as a high reflectance at target wavelength. Generally, thickness ratio of Mo layer in EUV multilayer is 0.4. 19.5 nm multilayer coating utilized in SUVI of GOES-R has a reflectance of larger than 25%, and a bandwidth of 1.1 nm due to an extremely small (0.15) thickness ratio of Mo layer. This Mo ratio is the smallest published value in 19.5 nm multilayer restricted by available physical thickness limits [4,5].

Although optical performance of Mo/Si is not the best, due to its good stable structure [8] and excellent optical properties, it was widely used in 13-35 nm [4,5]. Recently, some new multilayers were developed, such as Al/Zr, Al/Mo/SiC, Al/Mo/B_4C, and they also seem to show good stability [9-13]. Especially, Al/Mo/B_4C will be used in EUVI onboard ESA Solar Orbiter missions [14]. However, only Al/Zr has been suitably employed in the Hi-C sounding rocket experiment [15]. These new multilayers still need further strict examination. Si/Mo was chosen in our mirrors for their proved stability in long-term space missions.

X-EUV imager will be installed onto FengYun III satellite, which will be launched in 2020. It needs 19.5 nm multilayer coatings with a narrow bandwidth at normal (refer to normal coating) and 45° incidence (refer to 45° coating). In this paper, we will give the design, fabrication, characterization of 19.5 nm multilayer.

2 EUV optical system in X-EUV imager

EUV Imager and Spectrometer are two important components in X-EUV Imager. As shown in Figure 1a, EUV Imager has a Cassegrain structure with a spherical primary concave mirror and a spherical secondary convex mirror. Parallel light passes through window filter, it hits on the primary mirror, then it is

reflected by secondary mirror. Finally, it passes through central hole of primary mirror, and it is detected by CCD. The function of EUV Spectrometer is to monitor intensity variance of 19.5 nm, and it only detects line intensity. Thus, the requirements for surface figure and reflectance of the mirror in EUV Spectrometer are low. As shown in Figure 1b, parallel light passes through the filter, then it is reflected by two plane mirrors, and it is detected by CCD. To keep the structure compact, the incident angle of 45° is selected even though the reflectance is only half of normal incidence because 45° is roughly Brewster's angle in the EUV range. Although window filter can block most of unwanted lines, emission line near to 19.5 nm still can pass through window filter. Thus, multilayer mirror with a narrow band is required in EUV Imager and Spectrometer.

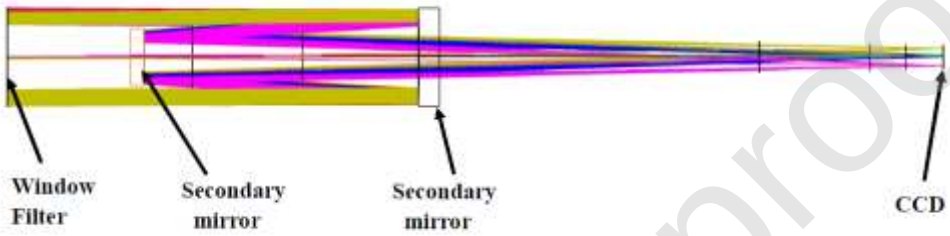

(a)

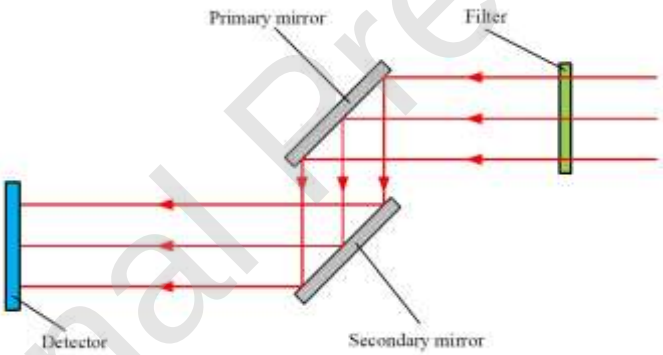

(b)

Figure 1 Ray trace of EUV Imager's optical system (a) with spherical primary and secondary mirrors and Spectrometer (b) with two plane mirrors in X-EUV Imager.

3 Design

Although Al-based mirrors seem to have good stability and better optical properties, they are lack of enough flight experience. Mo and Si are two widely used materials in EUV range due to their stability [8], the working wavelengths include 13.12, 17.11, 19.51, 28.42, and 30.38 nm [4,5,8]. Mo/Si multilayer has a good flight heritage in many Missions [4,5,8], such as SUVI [4], AIA [5], and Chang'e III [8]. Thus, we still select Mo and Si as material pair. To suppress adjacent lines (Fe VII, XI, XXI, and XIII), Mo/Si multilayer should have a narrow

bandwidth of less than 1.2 nm. Here the bandwidth refers to full width at half maximum (FWHM). The efficiency ratios between the unwanted and wanted lines in 8-35 nm for normal and 45° coatings are about 3% and 19%, respectively. The substrates are ZERODUR (6mm thickness) for normal coating and fused silica (3 mm thickness) for 45° coating with a roughness (RMS) of 0.7 nm. We employ IMD software to design 19.5 nm multilayer coatings with a narrow bandwidth at normal and 45° incidence [16]. The optical constants of Mo and Si are provided by Lawrence Livermore National Laboratory and the Center for X-Ray Optics in IMD software [17]. The design details are listed in Table 1. To obtain a narrow bandwidth, the Mo ratio of 0.15 is selected in normal coating, and an even smaller value of 0.11 is chosen in 45° coating.

Surface roughness and interlayer diffusion have a significant influence on spectral performance of EUV coatings because layer thickness is in a magnitude of several nanometers. Debye-Waller factor is introduced into calculation of reflectance as shown in Equation (1), and σ_j is roughness/diffusion, $\tilde{n}$ is complex refractive index, θ is incident angle, λ is wavelength. The real reflectance coefficient of multilayer is the ideal one multiplied by Debye-Waller [18-19].

(1) $$DW_j = \exp\left[-2\left(\frac{2\pi\sigma_j \tilde{n}_j \cos\theta_j}{\lambda}\right)^2\right]$$

Table 1 Design parameters of 19.5 nm Mo/Si multilayer coating for X-EUV Imager.

Incident angle	d (nm)	Periodic Number N	Γ_{Mo} (d_{Mo}/d)	Capping layer	Reflectance	Bandwidth (nm)
normal	10.1	30	0.15	3.5 nm Si	35.5%	1.0
45°	14.73	30	0.11	3.0 nm Si	20.0%	1.4

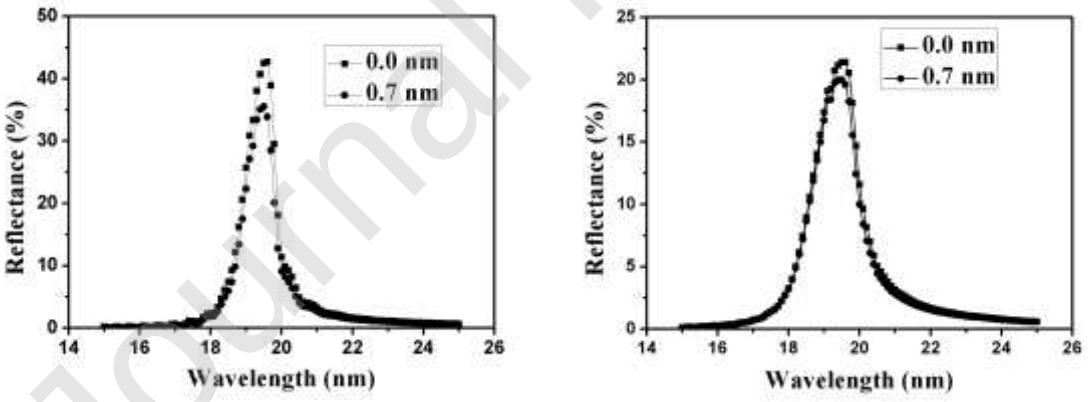

(a) **(b)**

Figure 2 The theoretical influence of surface roughness/diffusion on spectral performance of normal (a) and 45° (b) coatings.

Figure 2 theoretically shows the influence of surface roughness/diffusion on spectral performance of normal and 45° coatings, and surface roughness/interlayer diffusion is assumed to be 0.7 nm. For 45° coating, roughness leads to 6.6% loss of reflectance, for normal coating, roughness results

in 16.5% reduction of reflectance; which is nearly three times of the one for 45° coating. This phenomenon can be understood by Equation (1), and the influence of roughness on reflectance decreases with increasing of incident angle.

3 Fabrication and characterization methods

There are four sputtering sources in our deposition chamber, and they are configured in con-focal tilt mode, which is shown in Figure 3. We use two sources at diagonal position to deposit one material, and two sources is tilted at a angle α. This angle is tuned to obtain a good film thickness uniformity. The substrate is mounted at the center of four sources, and the height from the substrate to the source is about 10 cm. The substrate is rotated to achieve a good film thickness uniformity. The sources are fixed during deposition. No mask is used. The base pressure is better than 4.0×10^{-4} Pa, and working pressure is about 0.1 Pa. Mo and Si were deposited by DC magnetron sputtering, the power is 50 W for Mo, and 75 W for Si target. The thickness was controlled by time due to stable deposition rate in magnetron sputtering method. The deposition rate was about 0.05 nm/s.

Figure 3 Sputtering sources configured in con-focal tilt mode in our deposition chamber.

Spectral performance was measured by our developed laser-produced plasma (LPP) reflector, and the target is Copper. Figure 4 shows schematic diagram of our developed reflectometer, and IPC is the abbreviation of Interprocess Communication. Figure 5 shows an experimental setup of an EUV reflectometer. It is mainly composed of laser-produced copper plasma light source, EUV monochromator, sample's position controller, silicon photodiode, data acquisition system, and the sample chamber. For the LPP light source, the copper plasma is produced by Q-switch nanosecond pulsed laser at a wavelength of 1064nm, and a continuous spectrum of 10-40 nm is obtained. The EUV monochromator consists of a grazing incidence X-ray Czerny-Turner geometry and a wavelength controller for a 1200g/mm grating, its resolution is 0.1nm at FWHM. The detector subsystem consists of a photodiode and a signal processor that detects the intensity of the incident light. The sample is attached to the sample holder of the high-vacuum XYZ stage, and its position adjustment is

controlled by the servo motion system. During the measurement, the motion control system adjusts the position of the sample, the detector subsystem acquires the signal data, and the industrial computer realizes the automatic completion of the experimental process by virtue of the wavelength control, the data acquisition, and storage software. The error is ±2% in the reflectance measured by this reflectometer. The error is produced by noise, light source, monochromator, amplifier, calibration, and detector. The detector is calibrated by National Institute of Standards and Technology, and other errors are estimated by multiple measurements compared with the result of standard sample. Repeatability is influenced by stability of light source, rotation accuracy of grating, sample stage, detector, and noise. The LPP source is stable for a short time, but the test time is relatively long, and the relative change is still large, which will bring 1% signal change. The hollow diode detector monitor the fluctuation of the light source, and it is used to correct the results. Therefore, this process can reduce this change to 0.3%. Due to losing steps in the stepper motor, there is an error of 0.5% in the angle control, and a grating rotation error of 0.1%. All the rotation accuracies are monitored by the rotary encoder to restrain the rotation error. The combined error is less than 0.2% after adding the rotary encoders. The noise is an important factor affecting the repeatability when the signal-to-noise ratio is not high enough. Therefore, it is necessary to reduce external noise as much as possible. Generally, the signal-to-noise of the incident signal is relatively high. Thus, the impact is small. However, the signal-to-noise of the reflected signal is relatively low. All circuits have good shielding boxes with electrical grounding, and each of the circuit's power is supplied via a noise filter, and dark noise is tested in each measurement. Then it can reach 0.5% after the noise is reduced. Theoretically, the rms value is 0.62%. Finally, five measurements were performed to evaluate the repeatability of the measurement results, the repeatability is 0.83%.

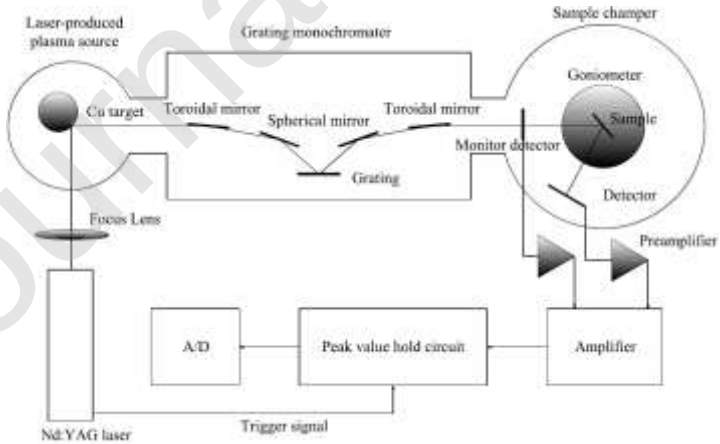

Figure 4 Schematic diagram of our developed reflectometer.

Figure 5 Experimental setup of our developed EUV reflectometer.

Stress is derived by changes of surface figure, and surface figure was measured by ZYGO GPI XP/D Interferometer. Grazing incidence of x-ray reflectance measurement (GIXRR) was conducted by X ray diffraction (XRD, DX-2000), and angular resolution is 0.005°. Surface roughness was characterized by Atomic Force Microscopy (AFM, Nanosurf C3000), scan area was 2μm×2μm, scan speed was 0.7 s/line, and measured point was 256 points/line.

4 Experimental results

4.1 Characterization

4.1.1 GIXRR

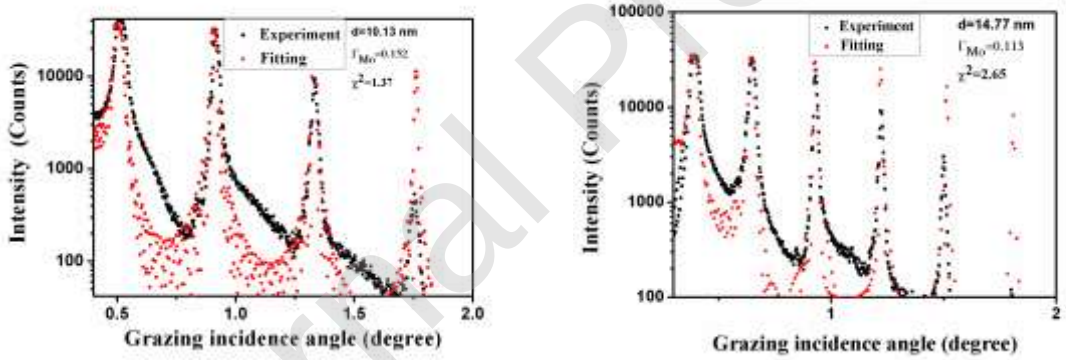

(a) (b)

Figure 6 GIXRR fittings of normal (a) and 45° (b) coatings.

Figure 6 shows GIXRR fittings of normal and 45°coatings, the periodic thicknesses are 10.13 nm and 14.77 nm, the Mo ratios are 0.152 and 0.113, respectively. The interface roughness is 0.7 nm. There are three and five sharp, strong XRD peaks, respectively, which indicates that there are distinct interfaces between Mo and Si layers and stable structure.

4.1.2 AFM

Figure 7 shows two dimensional (a1, b1) and three dimensional (a2, b2) AFM image of Mo/Si multilayer, and the scan area is 2 μm×2 μm. The roughness (Rq) is 0.7 (b)-0.73 (a) nm.

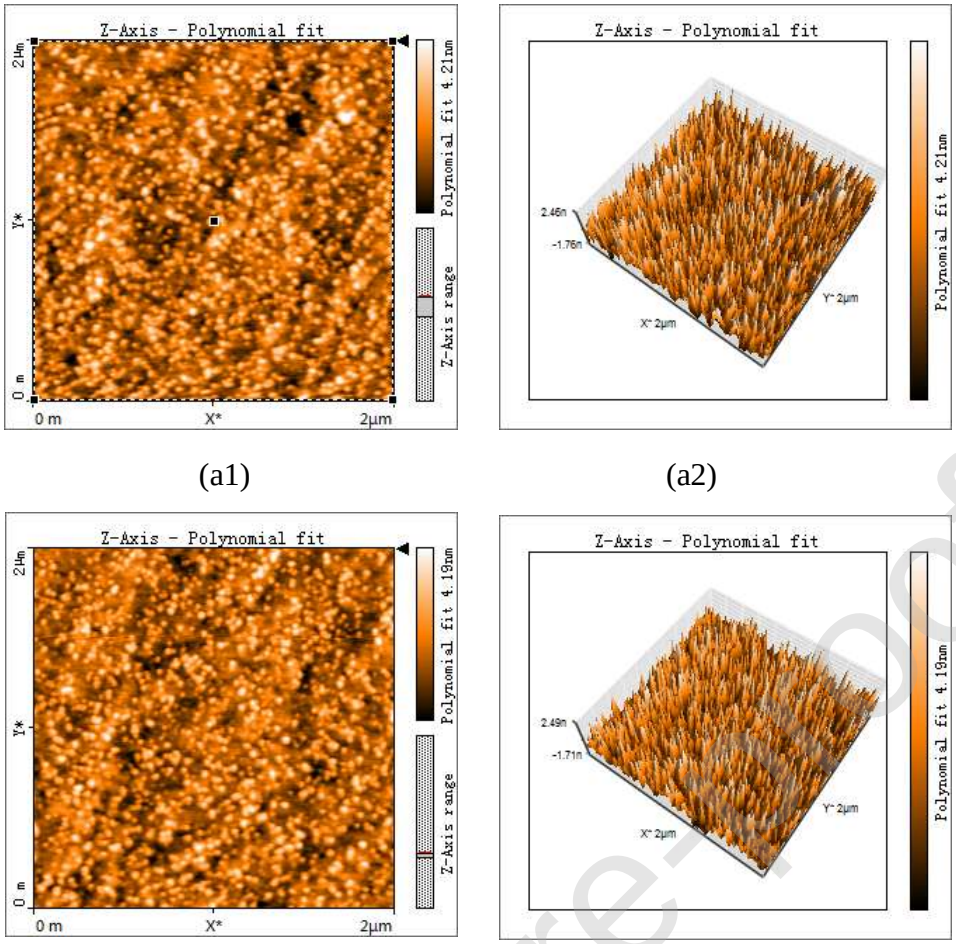

(a1) (a2)

(b1) (b2)

Figure 7 Two dimensional (a1, b1) and three dimensional (a2, b2) AFM image of Mo/Si multilayer

4.1.3 Reflectance

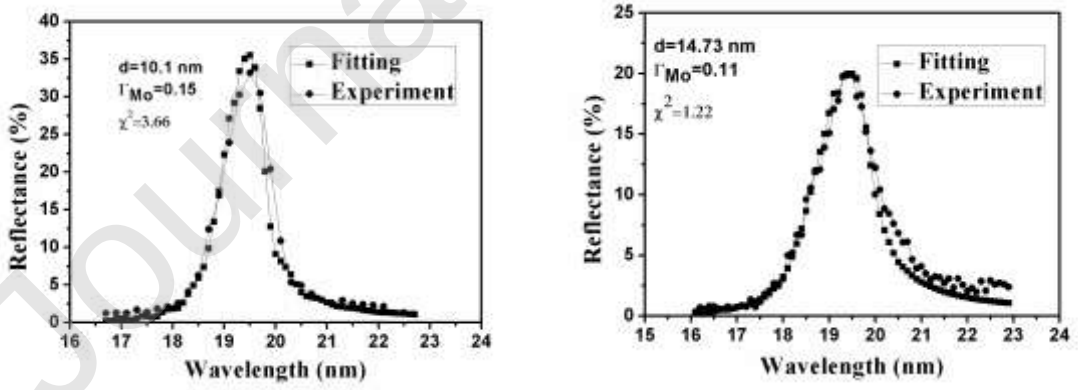

(a) **(b)**

Figure 8 Experimental reflectance curves of coatings (3° (a) and 45° (b)).

Reflectance measurement for normal coating was conducted at 3° incident angle. Figure 8 reveals experimental reflectance curves of coatings (3° (a) and 45° (b)).Theoretical fittings indicate that interface roughness/diffusion is about

0.7 nm. Experimental results demonstrate good agreements with theoretical fittings. They have reflectance of 33.2% and 19.8%, and bandwidth of 1.1 nm and 1.5 nm, respectively.

4.2 Stress

The stress can be derived by Stoney Equation [20]:

$$\sigma = \frac{E_s}{6(1-\upsilon_s)} \frac{t_s^2}{t_f} \left(\frac{1}{R} - \frac{1}{R_0} \right) \quad (2)$$

where E_s and v_s are Young's modulus and Poisson's ratio of the substrate; t_s and t_f are thicknesses of the substrate and film; and R_0 and R are the radii of curvature of the substrate before and after deposition. The concave surface figure refers to minus PV, and convex surface figure refers to positive PV. Young's modulus E_s and Poisson's ratio v_s are 9.1×10^{10} Pa and 0.24 for ZERODUR, and 7.17×10^{10} Pa and 0.17 for fused silica. The error of ZYGO GPI XP/D Interferometer is 0.01 wavelength, so error and uncertainty of the measurements is about 10%.

Table 2 Parameters for stress calculation of 19.5 nm coatings.

Incident angle	PV before	PV after	t_s	t_f	Diameter/effective aperture	Stress
normal	0.060 λ	0.029 λ	6 mm	306.5 nm	25 mm/89%	392 MPa
45°	-0.127 λ	0.142 λ	3 mm	441.9 nm	25 mm/86%	864 MPa

Table 2 provides parameters for stress calculations of 19.5 nm coatings. The stress for 45° coating is 864 MPa, which is two times for normal coating. Figure 9 demonstrates surface figure changes of normal (a) and 45° (b) coatings before (1) and after (2) deposition. For normal coating, before deposition, the shape of substrate is not isotropic, and there is three high points and two low points at the edge, the center is low. After deposition, three high points and two low points at the edge still exist, but the center gets higher. Thus, we just take accounts of the change between the three high points at the edge and the center into our stress calculation. Due to multilayer deposition, surface figures of substrate change from concave to convexity in 45° coating. This is because that Mo ratio (0.11) in 45° coating is smaller than the one (0.15) in normal coating. Due to high stress in 45° coating, the multilayer has potential delamination. No crake, delaminating phenomena, and reflectance drop were observed for 45° coating after one year, but it still needs further examination. In addition, 45° coating will be used in Spectrometer, and it does not involve imaging, and it just measures the light intensity of 19.5 nm. The requirements of surface figure and reflectance for 45° coating are low.

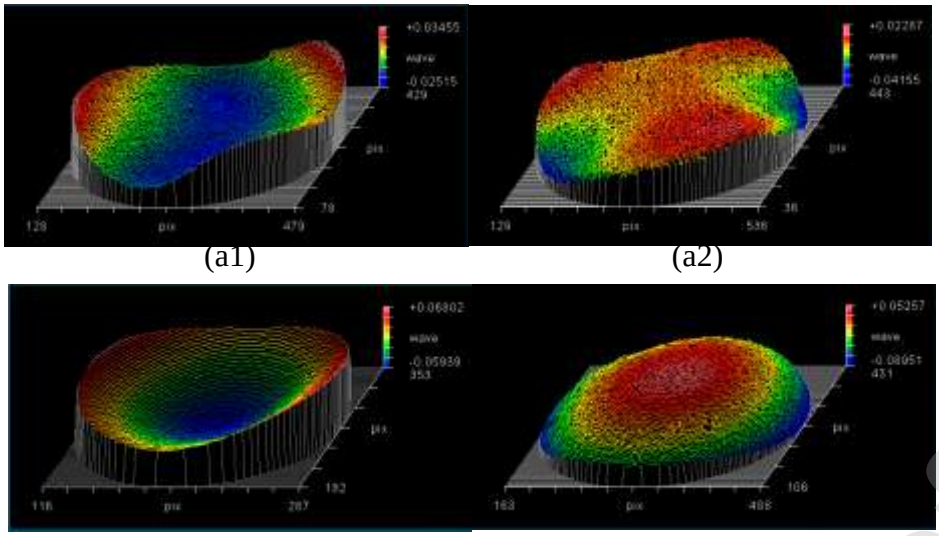

(a1) (a2)

(b1) (b2)

Figure 9 Surface figure changes of normal (a) and 45° (b) coatings before (1) and after (2) deposition.

5 Conclusions

19.5 nm coatings at normal and 45° incidence are designed, fabricated, and tested. They have reflectance of 33.2% and 19.8%, narrow bandwidth of 1.1 nm and 1.5 nm. It is found that the influence of roughness on the reflectance decreases with increasing of incident angles. The extreme small Mo ratio (0.11) results in high stress of 864 MPa. Our deposition system and developed reflectometer guarantee the success of fabrication of narrowband 19.5 nm coatings.

Declaration of interests

√ ☐ The authors declare that they have no known competing financial interests or personal relationships that could have appeared to influence the work reported in this paper.

Acknowledgments

This work is supported by the Joint Research Fund in Astronomy (U1531106, U1731114) under cooperative agreement between the National Natural Science Foundation of China (NSFC) and Chinese Academy of Science (CAS), partially supported by NSFC (Grant No.11427803), and partially supported by the Strategic Priority Research Program of Chinese Academy of Science (CAS), Grant No. XDA15320103.

References

1. L. Golub, E. Deluca, P. Hamilton, G. Nystrom, D. L. Windt, W. K. H. Schmidt, A. Dannenberg, A photometric imaging solar telescope, tunable in the extreme ultraviolet, utilizing multilayer x-ray optics, Rev. Sci. Instrum. **73**, 1908-1913 (2002).
2. J.-P. Delaboudinière et al., EIT: extreme-ultraviolet imaging telescope for the soho

mission, Sol. Phys. **162**, 291–312 (1995).
3. B. N. Handy, et al., Sol. Phys. **187**, 229-260 (1999).
4. D. M.-Galarce, R. Soufli, D. L. Windt, M. Bruner, E. Gullikson, S. Khatri, E. Spiller, J. C. Robinson, S. Baker, E. Prast, Multisegmented, multilayer-coated mirrors for the Solar Ultraviolet Imager, Opt. Eng. **52**, 095102 (2013).
5. R. Soufli, D. L. Windt, J. C. Robinson, S. L. Baker, E. Spiller, F. J. Dollar, A. L. Aquila, E. M. Gullikson, B. Kjornrattanawanich, J. F. Seely, L. Golub, Development and testing of EUV multilayer coatings for the atmospheric imaging assembly instrument aboard the Solar Dynamics Observatory, Proc. SPIE **5901**, 59010M (2005).
6. I. Yoshikawa, Telescope of extreme ultraviolet (TEX) onboard SELENE: science from the Moon, Earth Planets Space, **60**, 407–416 (2008).
7. Zhaohui Li, et al., Opto-mechanisms design of extreme-ultraviolet camera onboard Chang E lunar lander, Opt. Express 22, 15932 (2014).
8. Yunpeng Li, et al., Thermal and stress studies of the 30.4 nm Mo/Si multilayer mirror forthe moon-based EUV camera, Appl. Surf. Sci. **317**, 902–907 (2014).
9. D. L. Windt, EUV multilayer coatings for solar imaging and spectroscopy, Proc. SPIE **9604**, 96040P (2015).
10. A. J. Corso, M. G. Pelizzo, Extreme ultraviolet multilayer nanostructures and their application to solar plasma observations: a review, J. of nanosci. nanotechnol. **19** (1), 532-545 (2019).
11. Q. Zhong, W. Li, Z. Zhang, J. Zhu, Q. Huang, H. Li, Z. Wang, P. Jonnard, K. L. Guen, J. André, H. Zhou, T. Huo, Optical and structural performance of the Al(1%wtSi)/Zr reflection multilayers in the 17-19nm region, Opt. Express **20**, 10692-10700 (2012).
12. E. Meltchakov, S. D. Rossi, R. Mercier, F. Varniere, A. Jérome, F. Auchere, X. Zhang, M. Roulliay, F. Delmotte, Single and multi-channel Al-based multilayer systems for space applications in EUV range, Proc. SPIE **8777**, 87771C (2013)
13. E. Meltchakov, C. Hecquet, M. Roulliay, S. D. Rossi, Y. Menesguen, A. Jérome, F. Bridou, F. Varniere, M. F. Ravet-Krill, F. Delmotte, Development of Al-based multilayer optics for EUV, Appl. Phys. A **98**, 111-117 (2010).
14. J.-P. Halain, P. Rochus, E. Renotte, T. Appourchaux, D. Berghmans, L. Harra, U. Schühle, W. Schmutz, F. Auchère, A. Zhukov, C. Dumesnil, F. Delmotte, T. Kennedy, R. Mercier, D. Pfiffner, L. Rossi, J. Tandy, A. BenMoussa, P. Smith, The EUI instrument onboard the Solar Orbiter mission: from breadboard and prototypes to instrument model validation, Proc. SPIE 8443, 844307 (2012)
15. K. Kobayashi, J. Cirtain, A. R. Winebarger, K. Korreck, L. Golub, R. W. Walsh, B. De Pontieu, C. DeForest, A. Title, S. Kuzin, S. Savage, D. Beabout, B. Beabout, W. Podgorski, D. Caldwell, K. McCracken, M. Ordway, H. Bergner, R. Gates, S. McKillop, P. Cheimets, S. Platt, N. Mitchell, D. Windt, The High-Resolution Coronal Imager (Hi-C), Sol. Phys. **289**, 4393 (2014).
16. D. L. Windt, IMD—Software for modeling the optical properties of multilayer films, Comput. in Phys. **12**(4), 360-370 (1998).
17. http://www-cxro.lbl.gov/opticalIconstants.

18. D. G. Stearns, D. P. Gaines, D. W. Sweeney, E. M. Gullikson, Nonspecular X-ray scattering in a multilayer-coated imaging system, J. Appl. Phys. **84**, 1003-1028 (1998).
19. H. E. Bennett, J. O. Porteus, Relation between surface roughness and specular reflectance at normal incidence, J. Opt. Soc. Am. **51**, 123-129 (1961).
20. G. G. Stoney, The tension of metallic films deposited by electrolysis, Proc. R. Soc. London A **82**, 172–175 (1909).